The Astrophysical Journal Letters, 868:L30 (5pp), 2018 December 1 https://doi.org/10.3847/2041-8213/aaf0a5

Extreme-ultraviolet Radiation from A-stars: Implications for Ultra-hot Jupiters

L. Fossati[1], T. Koskinen[2], J. D. Lothringer[2], K. France[3,4], M. E. Young[1], and A. G. Sreejith[1]
[1] Space Research Institute, Austrian Academy of Sciences, Schmiedlstrasse 6, A-8042 Graz, Austria; luca.fossati@oeaw.ac.at
[2] Lunar and Planetary Laboratory, University of Arizona, 1629 East University Boulevard, Tucson, AZ 85721-0092, USA
[3] Laboratory for Atmospheric and Space Physics, University of Colorado, 600 UCB, Boulder, CO 80309, USA
[4] Center for Astrophysics and Space Astronomy, University of Colorado, 389 UCB, Boulder, CO 80309, USA
Received 2018 October 9; revised 2018 November 12; accepted 2018 November 13; published 2018 November 26

Abstract

Extremely irradiated, close-in planets to early-type stars might be prone to strong atmospheric escape. We review the literature showing that X-ray-to-optical measurements indicate that for intermediate-mass stars (IMSs) cooler than ≈8250 K, the X-ray and extreme-ultraviolet (XUV) fluxes are on average significantly higher than those of solar-like stars, while for hotter IMSs, because of the lack of surface convection, it is the opposite. We construct spectral energy distributions for prototypical IMSs, comparing them to solar. The XUV fluxes relevant for upper-planet atmospheric heating are highest for the cooler IMSs and lowest for the hotter IMSs, while the ultraviolet (UV) fluxes increase with increasing stellar temperature. We quantify the influence of this characteristic of the stellar fluxes on the mass loss of close-in planets by simulating the atmospheres of planets orbiting EUV-bright (WASP-33) and EUV-faint (KELT-9) A-type stars. For KELT-9b, we find that atmospheric expansion caused by heating due to absorption of the stellar UV and optical light drives mass-loss rates of $\approx 10^{11}$ g s^{-1}, while heating caused by absorption of the stellar XUV radiation leads to mass-loss rates of $\approx 10^{10}$ g s^{-1}, thus underestimating mass loss. For WASP-33b, the high XUV stellar fluxes lead to mass-loss rates of $\approx 10^{11}$ g s^{-1}. Even higher mass-loss rates are possible for less massive planets orbiting EUV-bright IMSs. We argue that it is the weak XUV stellar emission, combined with a relatively high planetary mass, which limit planetary mass-loss rates, to allow the prolonged existence of KELT-9-like systems.

Key words: planets and satellites: atmospheres – planets and satellites: gaseous planets – planets and satellites: individual (KELT-9b, WASP-33b) – stars: activity – stars: early-type

1. Introduction

Hot Jupiters (HJs) are subject to mass loss by hydrodynamic escape (e.g., Vidal-Madjar et al. 2003; Fossati et al. 2010). Hydrogen and helium in the upper atmosphere absorb high-energy and ionizing (X-ray and extreme-ultraviolet (XUV)) stellar radiation, leading to atmospheric heating and expansion, thus mass loss (Yelle 2004). Both approximations (Erkaev et al. 2007; Kubyshkina et al. 2018) and detailed hydrodynamic modeling (e.g., Koskinen et al. 2013a, 2013b, 2014) concur on values of the order of 10^{9-10} g s^{-1} for the mass-loss rates of classical HJs, e.g., HD209458b and HD189733b.

Atmospheric escape is a fundamental process affecting planetary atmospheric structure, composition, and evolution. For HJs, Szabó & Kiss (2011) and Mazeh et al. (2016) presented evidence for a lack of planets with orbital periods shorter than 1–2 days and masses smaller than one Jupiter mass (M_J) in the population of known exoplanets (i.e., sub-Jovian desert). Owen & Lai (2018) suggested that this might be the result of the interplay between atmospheric escape and planet migration.

Most exoplanets known to date orbit late-type stars, which are characterized by the presence of a chromosphere ($\approx 10^4$ K), a transition region ($\approx 10^5$ K), and a corona ($\approx 10^6$ K) lying on top of the photosphere. The XUV flux of late-type stars originates in these layers. There is, however, a rapidly increasing number of extremely irradiated HJs being detected around intermediate-mass stars (IMSs; main-sequence F5- to B5-type stars). Examples of such systems are WASP-33b, KELT-20b, WASP-189b, MASCARA-1b, and KELT-9b (Collier Cameron et al. 2010; Gaudi et al. 2017; Lund et al. 2017; Talens et al. 2017; Anderson et al. 2018). The *Transiting Exoplanet Survey Satellite* (*TESS*) mission is also expected to find several more of these systems (Barclay et al. 2018). Adequately estimating the XUV flux emitted by IMS is therefore critical for the determination of the physical characteristics and evolution of these extremely irradiated planets.

We review observational evidence indicating that the XUV flux of hotter IMSs provide a significantly different environment to their planets (Section 2) and use the information available to estimate the XUV fluxes of different IMSs. We then discuss the impact of these XUV fluxes on the atmosphere of HJs orbiting IMSs (Section 3) and present our conclusions in Section 4.

2. The High-energy Fluxes of IMSs

While there is a vast literature on the XUV fluxes of late-type stars, much less is known about those of IMSs. Stellar models suggest that the surface convection zone thins with increasing effective temperature ($T_{\rm eff}$) up to ≈8500 K (i.e., $B-V \approx 0.1$; spectral type A3), at which point it vanishes rapidly (e.g., Bohn 1984; Christensen-Dalsgaard 2000; Kupka & Montgomery 2002; Samadi et al. 2002). This theoretical prediction finds support in multi-wavelength observations.

Simon et al. (1995), Panzera et al. (1999), and Schröder & Schmitt (2007) analyzed *ROSAT* X-ray observations of a large sample of A-type stars. In general, they found an increasing number of X-ray detections with decreasing temperature. The results of Panzera et al. (1999) are representative. They considered a sample of 66 A- and 76 F-type stars ranging between spectral types A0 and F6 detected with *ROSAT*. By excluding binaries, for which the X-ray emission might come

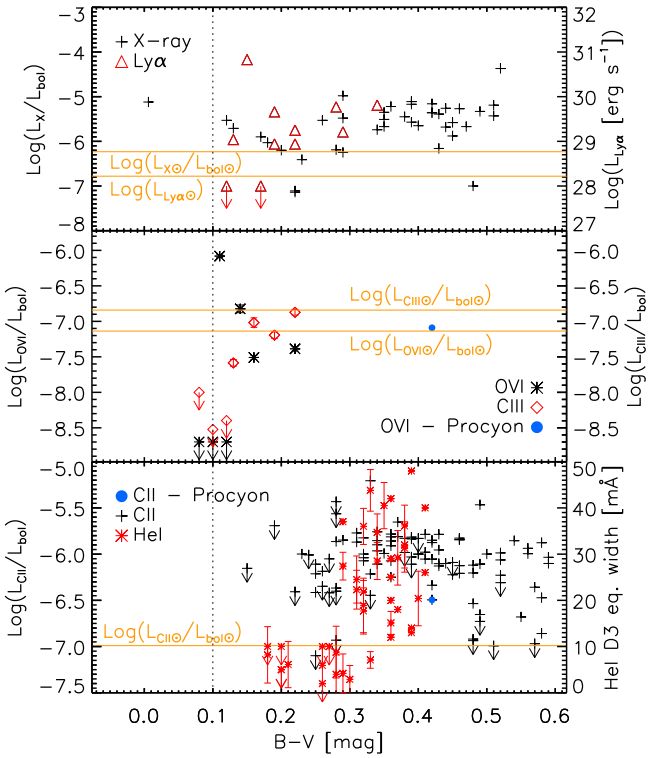

Figure 1. Top panel: X-ray luminosity (black plus sign; Panzera et al. 1999) and Lyα luminosity (red triangle; Marilli et al. 1997) vs. stellar $B-V$ color. The Lyα luminosities are not corrected for the bolometric luminosity because of a lack of data. Several early A-type stars are detected in the X-rays, but the emission comes from low-mass companions. Middle panel: O VI (black asterisk; Neff & Simon 2008) and C III (red rhombi; Simon et al. 2002) luminosity vs. $B-V$ color. Bottom panel: C II luminosity (black plus sign; Simon & Landsman 1991) and equivalent width of the He I D_3 line (red asterisk; Rachford 1997) vs. $B-V$ color. Downward arrows indicate upper limits. Horizontal lines mark solar values. The vertical line indicates the $B-V$ color at which stellar activity is believed to fade. In the middle and bottom panels, the blue dots indicate Procyon's O VI and C II luminosities. Lyα, O VI, C III, and C II emission and He I absorption are undetected for stars earlier than A3.

from the low-mass companion, they obtained a sample of 19 A- and 33 F-type stars showing X-ray emission, (almost) all later than spectral type A3 (Figure 1).

The *Extreme Ultraviolet Explorer* (*EUVE*) satellite collected extreme-ultraviolet (EUV; 70–760 Å) spectra of several nearby IMSs, but detecting just Procyon (F5) and Altair (A7; both also detected in X-rays; e.g., Simon et al. 1995), while no EUV emission was detected for Vega (A0; also undetected in X-rays; Schröder & Schmitt 2007), which is the nearest hot IMS (Craig et al. 1997). This indicates that Procyon and Altair have hot chromospheres and coronae, in contrast to Vega (Craig et al. 1997).

EUV radiation is heavily absorbed by the interstellar medium, therefore the search for and characterization of chromospheres and coronae on IMS can be better performed at far-ultraviolet (FUV; 912–1800 Å) wavelengths. This is because the FUV waveband contains emission lines with formation temperatures similar to those of the EUV emission (i.e., $10^{5\text{-}6}$ K). Simon & Landsman (1991), Schrijver (1993), Simon et al. (1994), and Walter et al. (1995) showed that the C II (1335 Å) emission flux of early F-type stars can be as high as that of the most active late-type dwarfs. Furthermore, Lyα emission is clearly detected in stars only up to spectral type A4 (e.g., Marilli et al. 1997; Simon et al. 2002).

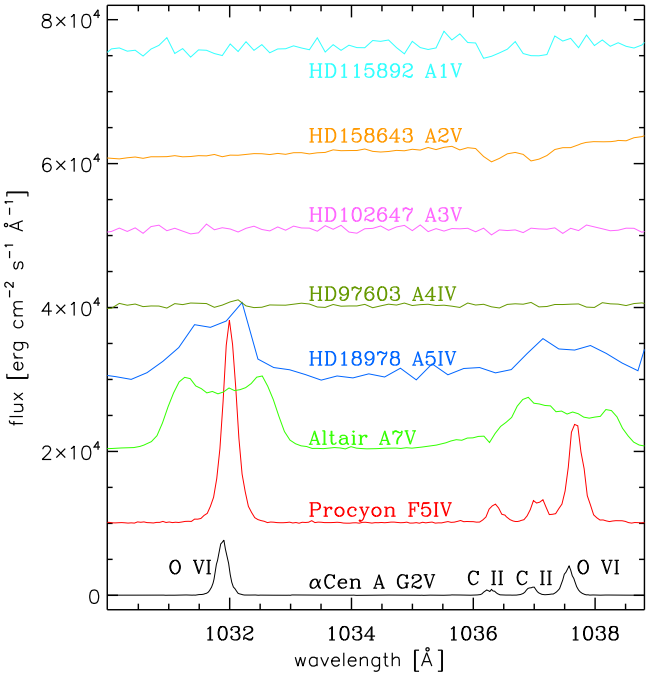

Figure 2. *FUSE* surface fluxes in the region of the C II 1036 and 1037 Å and of the O VI 1032 and 1037 Å lines for G2- to A1-type stars. We applied rigid shifts and rebinning for visualization purposes. The O VI emission disappears abruptly around spectral type A4–A5. The C II emission turns into absorption for the hotter stars. Altair and HD18978 are fast rotators, hence the broad emission lines.

Observations at wavelengths longer than Lyα (1216 Å) are limited to the cooler IMSs because the diagnostic lines (e.g., C II 1335 Å, Si IV 1400 Å, C IV 1550 Å) become harder to detect against the photospheric background rising with increasing $T_{\rm eff}$. By lying at shorter wavelengths, the spectral region blueward of Lyα (912–1200 Å) is less affected by stellar continuum emission up to the early A-type stars. Simon et al. (2002) and Neff & Simon (2008) reported measurements of the chromospheric and transition region emission lines C III (977 Å), O VI (1032 and 1037 Å), and C III (1175 Å) obtained from the *Far Ultraviolet Spectroscopic Explorer* (*FUSE*) spectra for a set of seven nearby IMSs in the 7800–8600 K $T_{\rm eff}$ range (i.e., A7–A2). They found strong emission lines for stars with $T_{\rm eff} \leqslant 8200$ K (A4), beyond which no line emission is detected (Figure 2). They also showed that the O VI luminosity correlates tightly with the X-ray luminosity, as expected for an emission generated by hot chromospheric and coronal material.

It is also possible to gather information about chromospheric and coronal properties of IMSs from observations in the optical band. The He I D_3 (5876 Å) absorption line is a classical activity indicator, present in stars with chromospheres (e.g., Wolff & Heasley 1984). Garcia-Lopez et al. (1993) and Rachford (1997) collected spectra for about 50 IMSs concluding that the line appears to be present for stars later than A5 and that the line strength is independent of rotation and age.

Multi-wavelength measurements (Figure 1) concur on the presence of a sharp boundary at 8000–8500 K, where cooler stars present chromospheres and coronae, thus high XUV fluxes, while hotter stars do not. These measurements also indicate that the XUV emission of cooler IMSs is likely to be significantly stronger than that of inactive late-type stars like the Sun. This is confirmed by comparing the XUV fluxes of

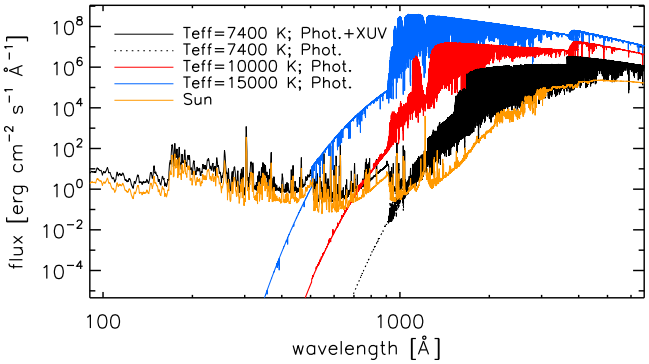

Figure 3. Comparison between non-LTE SEDs computed for IMSs with temperatures of 7400 K (black) and 10,000 K (red), and for the Sun (orange) and a 15,000 K star (blue). For the cooler IMSs, we used the XUV fluxes of Procyon at wavelengths below 1100 Å, while the photospheric fluxes are shown by the dashed line. All fluxes are scaled to a distance of 0.03 au and account for the radii typical of stars with the respective temperatures.

Procyon and solar (Fossati et al. 2018), showing that the former are about three times higher than the latter.

To estimate the impact of the presence/lack of XUV irradiation on the atmosphere of close-in planets orbiting IMSs, we computed spectral energy distributions (SEDs) for a 7400 K star (similar to WASP-33) and a 10,000 K star (similar to KELT-9), thus for stars with and without a chromosphere/corona, employing the non-local thermodynamic equilibrium (LTE) *PHOENIX* stellar model atmosphere code, v15 (Hauschildt & Baron 1999, Figure 3). In this comparison, we further consider the Sun and a $T_{\rm eff} = 15{,}000$ K star because planets are in principle detectable with *TESS* orbiting such high-temperature stars (Bouma et al. 2017). We rescaled all fluxes to a distance of 0.03 au, i.e., in between the orbital separations of WASP-33b and KELT-9b (Collier Cameron et al. 2010; Gaudi et al. 2017). For the cooler IMSs, we assumed that the XUV flux below 1100 Å is similar to that of Procyon. However, Figure 1 indicates that Procyon's XUV flux might be underestimating that of a 7400 K star. Table 1 quantifies the short-wavelength emission of the considered stars.

Based on the evidence presented here, cooler IMSs have strong XUV fluxes at wavelengths shorter than the hydrogen ionization threshold (912 Å) that are relevant to heating the upper atmospheres of giant planets orbiting IMSs, hereafter ultra-hot Jupiters (UHJs; Figure 3; Table 1). In contrast, the XUV flux of hotter IMSs decreases rapidly with decreasing wavelength, with ≈99% of the hydrogen ionizing radiation confined between 750 and 912 Å, making the XUV fluxes below 750 Å, the more relevant for driving planet atmospheric escape (see below), negligible compared to those of the other stars. The hotter IMSs, however, have the strongest FUV and NUV (1800–3200 Å) fluxes. We expect that this difference in the SEDs of IMSs has interesting consequences for the heating and escape of UHJs.

3. Implications for Exoplanets

The possible difference in XUV fluxes from cooler to hotter IMSs would have profound implications for atmospheric modeling and interpretation of the observations of UHJs. This is especially true for upper atmosphere observations and mass-loss predictions. Current models of UHJ atmospheres show that stellar continuum fluxes produce high temperatures leading to the dissociation of molecules and thermal ionization of low-ionization threshold metals such as Si, Mg, Fe, Na, and K at relatively high pressures ($p > 1$ μbar) compared to classical HJs (Kitzmann et al. 2018; Lothringer et al. 2018; Parmentier et al. 2018). In particular, only simple diatomic molecules (e.g., H_2, CO, OH) may survive in the upper atmosphere ($p < 1$ mbar) with detectable abundances.

Lothringer et al. (2018) and Kitzmann et al. (2018) suggested that CO infrared bands would be detectable in the spectra of UHJs with the *James Webb Space Telescope* (*JWST*). Given the high photospheric FUV fluxes of hot IMSs, the FUV bands of CO (van Dishoeck & Black 1988) may also be detectable during primary transit. The alkali atom lines in the optical that are prominent features in the transmission spectrum of classical HJs, on the other hand, should be significantly muted by ionization around the 10–100 mbar level. Metal opacities (Fe and Mg) and absorption from SiO, metal hydrates, and H^-, which is the main infrared opacity source in UHJs, lead to the formation of a temperature inversion in the lower atmosphere, which is present even without invoking TiO and VO absorption (Lothringer et al. 2018).

KELT-9b is the hottest of the known UHJs and as such it presents a fascinating test case for mass-loss studies. The energy limit for mass loss is given by Erkaev et al. (2007)

$$\dot{M} = \frac{\pi \epsilon F_{\rm XUV} r^2}{\Phi_0 K} \left(\frac{R_{\rm s}}{a} \right) \quad (1)$$

where ϵ is the heating efficiency, $F_{\rm XUV}$ is the stellar surface XUV flux, Φ_0 is the gravitational potential at the planetary radius, r is the effective radius in the atmosphere where the XUV flux is absorbed, $R_{\rm s}$ is the stellar radius, a is the orbital semimajor axis, and K accounts for Roche lobe effects and depends on the ratio of the L1 point radius to the planetary radius. Assuming the XUV flux value from Table 1 for a 10,000 K star, energy-limited escape from KELT-9b would be $\approx 10^{11}$ g s^{-1}. However, this value is based on 100% heating efficiency, which is too high. To highlight this effect, we arbitrarily consider a reference wavelength of 750 Å (see Table 1), which is the approximate position at which the fluxes of the star with $T_{\rm eff} = 10{,}000$ K cross those of the star with $T_{\rm eff} = 7400$ K. As the heating efficiency increases with photon energy up to a point where the photoelectron reaches the ionization potential of hydrogen, the heating efficiency for ionizing radiation at wavelengths longer than 750 Å (i.e., where most of the stellar XUV flux is emitted) is ≈10%, thus the energy-limited mass-loss rate is probably closer to 10^{10} g s^{-1}. This result is independent of the considered reference wavelength, because at wavelengths longer than 750 Å the XUV fluxes are higher, but the heating efficiency is lower, while at shorter wavelengths it is the opposite. This is the result of the strong wavelength dependency of the XUV fluxes of hot IMSs with wavelength, which is instead not the case for late-type stars. Given that detailed calculations addressing the contribution of the longer wavelength FUV radiation to the energy budget of the upper atmosphere do not exist, at this stage it is acceptable to assume an energy-limited escape rate of 10^{10}–10^{11} g s^{-1}.

We note that the energy limit based on the XUV flux is not adequate for predicting mass-loss rates for UHJs due to the dissociation of molecules, including H_2, at deeper pressures

Table 1
Comparison between the Integrated XUV, FUV, and Near-ultraviolet (NUV) Fluxes Obtained for the Stars Shown in Figure 3

Star	XUV <912 Å (<750 Å) (erg cm^{-2} s^{-1})	FUV 912–1800 Å (erg cm^{-2} s^{-1})	NUV 1800–3000 Å (erg cm^{-2} s^{-1})	$\frac{\text{XUV}}{\text{FUV}}$	$\frac{\text{XUV}}{\text{FUV}+\text{NUV}}$
10,000 K	4000 (60)	6×10^{9}	1×10^{10}	7×10^{-7} (1×10^{-8})	2×10^{-7} (3×10^{-9})
7400 K	7800 (6500)	3×10^{7}	1×10^{9}	2×10^{-4} (2×10^{-4})	7×10^{-6} (6×10^{-6})
Sun	2400 (2000)	3×10^{4}	3×10^{7}	1×10^{-1} (8×10^{-2})	8×10^{-5} (7×10^{-5})
15,000 K	6×10^{6} (4×10^{5})	2×10^{11}	1×10^{11}	3×10^{-5} (2×10^{-6})	2×10^{-5} (1×10^{-6})

Note. The integrated fluxes are in erg cm^{-2} s^{-1} and are for a distance of 0.03 au. Values in parenthesis are for fluxes below 750 Å. The last two columns give flux ratios comparing the XUV and FUV or FUV+NUV.

than on classical HJs (T. Koskinen et al. 2018, in preparation). To illustrate this point, we use the model of Lothringer et al. (2018) to estimate the mass-loss rate for KELT-9b. To do so, we calculate the extent of the atmosphere based on the predicted T-P profile and composition, including the effect of the Roche potential and assuming that energy is fully redistributed around the planet. We find that the pressure of the Roche lobe equipotential surface is about 10^{-11} bar. Given that the effective thermal escape parameter approaches zero at the Roche lobe boundary, Jeans escape reduces to the "free particle" (sound speed) limit and we find a mass-loss rate of 10^{10}–10^{11} g s^{-1} i.e., comparable to the energy limit. This mass-loss rate is almost entirely powered by the expansion of the atmosphere due to the heating of the middle and upper atmosphere by UV and visible radiation, while XUV thermospheric heating has only a small effect on the T-P profile.

Casasayas-Barris et al. (2018) presented results of high-resolution optical transmission spectroscopy of the UHJ MASCARA-2b, including the detection of Na and Hα absorption. Hydrogen absorption at the position of the Hα line has been detected in transmission also for the UHJ KELT-9b (Yan & Henning 2018). Both of these planets orbit IMSs with temperatures well above the 8000–8500 K threshold. We used the model results from Lothringer et al. (2018) to estimate the magnitude of KELT-9b Hα absorption, assuming LTE-level populations for hydrogen, similar to Yan & Henning (2018) and Casasayas-Barris et al. (2018). We find that the abundance of the $n = 2$ population peaks around 0.2 μbar, with a mixing ratio of about 10^{-8}, in line with the relatively high temperature of about 6000 K at that pressure level. This leads to a Hα core transit depth of about 1.2%.

Our results show that a significant excess transit depth over the continuum transit depth of ≈0.7% can be produced without invoking strong additional mass loss by XUV radiation. This conclusion agrees qualitatively with the results of Casasayas-Barris et al. (2018) for MASCARA-2b. Our calculated transit depth of KELT-9b, however, falls short of the observed Hα transit depth of 1.8% (Yan & Henning 2018). There are several possible reasons for this discrepancy. The atmosphere could be hotter and more extended than we predicted, leading to a larger transit depth and higher mass-loss rate. The significant mass uncertainty ($2.88 \pm 0.84\,M_{\rm J}$ Gaudi et al. 2017) can also contribute to the discrepancy. If the true planetary mass is closer to the lower end of the 1σ range, the atmosphere would be more extended with a larger transit depth and higher mass-loss rate, without the need to increase the temperature.

It would be possible to explore different temperature profiles and planet masses to obtain a better fit with the observations, but this exercise, however, is not particularly informative at this point for two main reasons. First, the current uncertainties in the system properties preclude strong conclusions on mass loss based on the existing observations. Second, the hydrogen $n = 2$ level population in the upper atmosphere likely deviates significantly from LTE. Detailed calculations of level populations have been undertaken on classical HJs (Menager et al. 2013; Huang et al. 2017), but have not been extended to UHJs and are outside of the scope of this Letter. They do indicate, however, that the inclusion of radiative and photoelectron excitation could potentially enhance the $n = 2$ level population.

Yan & Henning (2018) employed the information derived from the depth of the Hα line of KELT-9b to infer a planetary mass-loss rate of about 10^{12} g s^{-1}, assuming Jeans escape. They then mentioned that this value might be underestimated, because it ignores escape driven by the stellar XUV flux. In fact, both Casasayas-Barris et al. (2018) and Yan & Henning (2018), who regarded hot IMSs as if they would have XUV fluxes stronger than those of solar-like stars, interpreted the Hα absorption as being the result of excitation due to XUV absorption. Instead, we argue that the mass-loss rate derived by Yan & Henning (2018) could be close to correct or even higher than the real mass-loss rate, because the star lacks strong emission at the wavelengths most relevant for driving escape that is not necessarily required to explain the existing transit observations.

As indicated by Table 1, UHJs orbiting cool IMSs, such as WASP-33b, are instead probably subject to XUV irradiation significantly larger than that of classical HJs. The EUV flux is absorbed by hydrogen and helium in the upper atmosphere while X-rays and UV radiation are absorbed by metals in the lower atmosphere. This implies that planets orbiting cool IMS could undergo significant heating across the whole atmosphere that will lead to powerful hydrodynamic escape, possibly one or more orders of magnitude larger than that of classical HJs. This, however, does not appear to be the case for WASP-33b, where the energy-limited mass-loss rate is $\approx 10^{11}$ g s^{-1} based on the XUV flux given in Table 1 and heating in the middle atmosphere does not add significantly to the mass loss rate. In contrast to planets orbiting cooler IMSs, planets orbiting hot IMSs may be subject almost exclusively to UV irradiation, which is absorbed by metals. As a result, the available energy to heat the thermosphere is much smaller and mass-loss rates are suppressed unless the planet is also subject to significant Roche lobe overflow. From the planet's perspective, the most threatening scenario is Roche lobe overflow partly powered by UV and visible radiation combined with significant XUV fluxes, which we argue is not the case for KELT-9b, providing

a compelling explanation for the detection of a planet in such an extreme environment in the first place.

4. Conclusions

We reviewed past X-ray, EUV, UV, and optical observations of IMSs showing the split nature of their XUV emission. For the cooler IMSs, the XUV fluxes, particularly those most relevant for driving planet atmospheric escape (<750 Å), are on average significantly higher than those of solar-like stars, while for the hotter IMS later than mid B-type it is the opposite. Observations concur at setting the threshold at ≈8250 K.

We estimated the impact of the XUV fluxes peculiar behavior on the atmospheric escape of UHJs. We concluded that the energy-limited approach alone is not applicable to many UHJs, as it may underestimate escape rates. For KELT-9b, which is subject to low XUV but high UV irradiation levels, we found XUV-driven mass-loss rates of $\approx 10^{10}$–10^{11} g s^{-1}, while atmospheric expansion caused by heating due to absorption of the stellar UV and optical light alone leads to similar mass-loss rates. For UHJs orbiting cooler IMSs, such as WASP-33b, the strong XUV stellar fluxes power mass-loss rates of $\approx 10^{11}$ g s^{-1}, though they could be even higher because of the additional heating of the middle atmosphere.

The weak emission at wavelengths shorter than 750 Å for the hotter IMS and the relatively high mass of the planet may explain why the atmosphere of KELT-9b has not completely escaped. Therefore, the planet should not be in a short-lived phase of evolution, hence more KELT-9b-like planets might exist. The generally high mass-loss rates we estimated for UHJs indicate that atmospheric escape plays a pivotal role in shaping their evolution and that UHJs are ideal laboratories to study escape.

The stellar EUV fluxes are a key ingredient for future mass-loss studies of UHJs. However, observations at EUV wavelengths have not been possible because the decommissioning of the *EUVE* satellite. Additionally, the modest aperture and low-throughput of *EUVE* limited it to only the nearest low- and IMSs. A new EUV mission featuring higher sensitivity (effective area >50 cm^2)[5] could overcome these prior limitations to survey EUV emission from a statistical sample of stars within 30 pc, placing exoplanet mass-loss observations on a firmer empirical basis.

L.F. and A.G.S. acknowledge support from FFG-P859718. We thank the anonymous referee for useful comments.

ORCID iDs

L. Fossati https://orcid.org/0000-0003-4426-9530
J. D. Lothringer https://orcid.org/0000-0003-3667-8633
K. France https://orcid.org/0000-0002-1002-3674

[5] The peak *EUVE* effective area was 2 cm^2 (https://archive.stsci.edu/euve/handbook/handbook.html).

References

Anderson, D. R., Temple, L. Y., Nielsen, L. D., et al. 2018, MNRAS, submitted (arXiv:1809.04897)
Barclay, T., Pepper, J., & Quintana, E. V. 2018, ApJS, 239, 2
Bohn, H. U. 1984, A&A, 136, 338
Bouma, L. G., Winn, J. N., Kosiarek, J., & McCullough, P. R. 2017, arXiv:1705.08891
Casasayas-Barris, N., Palle, E., Yan, F., et al. 2018, A&A, 616, A151
Christensen-Dalsgaard, J. 2000, in ASP Conf. Ser. 210, Delta Scuti and Related Stars, ed. M. Berger & M. Montgomery (San Francisco, CA: ASP), 187
Collier Cameron, A., Guenther, E., Smalley, B., et al. 2010, MNRAS, 407, 507
Craig, N., Abbott, M., Finley, D., et al. 1997, ApJS, 113, 131
Erkaev, N. V., Kulikov, Y. N., Lammer, H., et al. 2007, A&A, 472, 329
Fossati, L., Haswell, C. A., Froning, C. S., et al. 2010, ApJL, 714, L222
Fossati, L., Koskinen, T., France, K., et al. 2018, AJ, 155, 113
Garcia-Lopez, R. J., Rebolo, R., Beckman, J. E., & McKeith, C. D. 1993, A&A, 273, 482
Gaudi, B. S., Stassun, K. G., Collins, K. A., et al. 2017, Natur, 546, 514
Hauschildt, P. H., & Baron, E. 1999, JCoAM, 109, 41
Huang, C., Arras, P., Christie, D., & Li, Z-Y. 2017, A&A, 851, 150
Kitzmann, D., Heng, K., Rimmer, P. B., et al. 2018, ApJ, 863, 183
Koskinen, T. T., Harris, M. J., Yelle, R. V., & Lavvas, P. 2013a, Icar, 226, 1678
Koskinen, T. T., Lavvas, P., Harris, M. J., & Yelle, R. V. 2014, RSPTA, 372, 20130089
Koskinen, T. T., Yelle, R. V., Harris, M. J., & Lavvas, P. 2013b, Icar, 226, 1695
Kubyshkina, D., Fossati, L., Erkaev, N., et al. 2018, ApJL, 866, L18
Kupka, F., & Montgomery, M. H. 2002, MNRAS, 330, L6
Lothringer, J. D., Barman, T., & Koskinen, T. 2018, ApJ, 866, 27
Lund, M. B., Rodriguez, J. E., Zhou, G., et al. 2017, AJ, 154, 194
Marilli, E., Catalano, S., Freire Ferrero, R., et al. 1997, A&A, 317, 521
Mazeh, T., Holczer, T., & Faigler, S. 2016, A&A, 589, A75
Menager, H., Barthélemy, M., Koskinen, T., et al. 2013, Icar, 226, 1709
Neff, J. E., & Simon, T. 2008, ApJ, 685, 478
Owen, J. E., & Lai, D. 2018, MNRAS, 479, 5012
Panzera, M. R., Tagliaferri, G., Pasinetti, L., & Antonello, E. 1999, A&A, 348, 161
Parmentier, V., Line, M. R., Bean, J. L., et al. 2018, A&A, 617, A110
Rachford, B. L. 1997, ApJ, 486, 994
Samadi, R., Goupil, M.-J., & Houdek, G. 2002, A&A, 395, 563
Schrijver, C. J. 1993, A&A, 269, 446
Schröder, C., & Schmitt, J. H. M. M. 2007, A&A, 475, 677
Simon, T., Ayres, T. R., Redfield, S., & Linsky, J. L. 2002, ApJ, 579, 800
Simon, T., Drake, S. A., & Kim, P. D. 1995, PASP, 107, 1034
Simon, T., & Landsman, W. 1991, ApJ, 380, 200
Simon, T., Landsman, W. B., & Gilliland, R. L. 1994, ApJ, 428, 319
Szabó, G. M., & Kiss, L. L. 2011, ApJL, 727, L44
Talens, G. J. J., Albrecht, S., Spronck, J. F. P., et al. 2017, A&A, 606, A73
van Dishoeck, E. F., & Black, J. H. 1988, ApJ, 334, 771
Vidal-Madjar, A., Lecavelier des Etangs, A., Désert, J.-M., et al. 2003, Natur, 422, 143
Walter, F. M., Matthews, L. D., & Linsky, J. L. 1995, ApJ, 447, 353
Wolff, S. C., & Heasley, J. N. 1984, PASP, 96, 231
Yan, F., & Henning, T. 2018, NatAs, 2, 714
Yelle, R. V. 2004, Icar, 170, 167